Energy Conversion and Management 165 (2018) 578–592

Contents lists available at ScienceDirect

Energy Conversion and Management

journal homepage: www.elsevier.com/locate/enconman

Roads to improve the performance of hybrid thermosolar gas turbine power plants: Working fluids and multi-stage configurations

M.J. Santos, C. Miguel-Barbero, R.P. Merchán, A. Medina*, A. Calvo Hernández

Department of Applied Physics, University of Salamanca, 37008 Salamanca, Spain

ARTICLE INFO

Keywords:
Thermosolar hybrid plants
Multi-stage Brayton
Overall efficiency
Improved pre-design

ABSTRACT

This paper presents a general thermodynamic model for hybrid Brayton central tower thermosolar plants. These plants have been proved to be technically feasible but research and development efforts need to be done in order to improve its commercial interest. From the thermodynamic viewpoint it is necessary to increase its performance to get larger power production with reduced fuel consumption, and so reduced emissions. A model for multi-step compression and expansion is developed with that aim. The model is flexible and allows to simulate recuperative or non-recuperative plants, with an arbitrary number of stages and working with different subcritical fluids. The results for multi-step configurations are compared with those obtained for a plant with one turbine and one compressor. Different working fluids are analyzed, including air, nitrogen, carbon dioxide, and helium. Several plant layouts and the corresponding optimal pressure ratios are analyzed. Configurations with two-stages compression with intercooling combined with one or two expansion stages can significantly improve overall plant efficiency and lower fuel consumption. Power block efficiencies can reach 0.50 and overall plant efficiency can attain values about 0.40 working with air or carbon dioxide. For instance, comparing with a single-stage plant running with air, a plant working with subcritical carbon dioxide and two compression stages with intercooling can reach an overall efficiency about 19% larger and a fuel conversion rate around 23% larger. For such configuration, the specific fuel consumption is predicted to be about 108 kg/(MW h) at design point conditions.

1. Introduction

Concentrating solar power (CSP) is one of the promising renewable energy technologies that can contribute to decrease the dependence on fossil fuels for the generation of electricity and so, the environmental impact of energy production. As mentioned by Nathan et al. [1], unlike other renewable resources this technology is suited to produce non-intermittent power with the implementation of thermal storage. Peterseim et al. [2] discuss which CSP technologies are best suited for hybridization. Powell et al. [3] have recently published an extensive work on hybridization possibilities, including geothermal and photovoltaic resources. In this work CSP plants in which solar heat input is complemented with the heat released by the combustion of natural gas in a combustion chamber are surveyed. This technology ensures an almost constant energy injection to the grid in the range of a few megawatts. These plants are not completely free of fossil fuel consumption and pollutant emissions but guarantee predictability. Olumayegun et al. [4] highlight that the plants which work following a closed Brayton-like thermal cycle require a reduced water consumption compared with those working on Rankine cycles and can reach similar efficiencies. This point is especially advantageous in arid regions with appropriate solar resources. To get those efficiencies quite high turbine inlet temperatures have to be reached in the solar receivers, about 800–1000 °C. Several experimental prototypes [5] have shown that this is feasible using ceramic materials in central tower volumetric receivers. Ho and Iverson [6] have summarized these advances. Pioneer demonstration size plants have arrived at the same conclusion: the technology is practicable but it is still necessary a R&D activity to look for ways to improve the overall plant efficiency in order to get commercially interesting levelized costs of electricity, as pointed out by Korzynietz et al. [7]. Particularly, as mentioned by Dunham and Iverson [8], thermo-economic studies show that there is still a wide margin for improvement in the power block.

Along this work line thermodynamic studies about possible refinements on the basic Brayton cycle and the effects of the working fluid are important to guide future plant designs, as stated by Osorio et al. [9]. McMahan et al. [10] modelled the plant in terms of a reduced number of parameters. Within a similar framework, Zare and Hasanzadeh [11]

* Corresponding author.
E-mail addresses: smjesus@usal.es (M.J. Santos), cesarmi@usal.es (C. Miguel-Barbero), rpmerchan@usal.es (R.P. Merchán), amd385@usal.es (A. Medina), anca@usal.es (A. Calvo Hernández).

https://doi.org/10.1016/j.enconman.2018.03.084
Received 12 December 2017; Received in revised form 20 March 2018; Accepted 26 March 2018

Nomenclature

A_a	aperture area of the solar field (m^2)
A_r	solar receiver area (m^2)
a_c	isentropic compressor pressure ratio
a_t	isentropic turbine pressure ratio
C	solar collector concentration ratio
c_w	specific heat of the working fluid [J/(mol K)]
f	solar share
G	direct solar irradiance (W/m^2)
h_1	radiation heat loss coefficient for the solar collector (K^{-4})
h_2	effective convection and conduction loss coefficient for the solar collector (K^{-1})
$\dot{m}$	mass flow rate of the working substance (kg/s)
$\dot{m}_f$	fuel mass flow rate in the main combustion chamber (kg/s)
$\dot{m}_{fi}$	fuel mass flow rate in reheaters (kg/s)
P	power output (W)
$\lvert\dot{Q}_C\rvert$	heat losses at the combustion chamber (W)
$\lvert\dot{Q}_H\rvert$	total heat-transfer rate absorbed from the working fluid (W)
$\lvert\dot{Q}_{iHC}\rvert$	heat losses at the heat exchanger associated to the combustion chamber (W)
$\lvert\dot{Q}_{HC}\rvert$	heat rate input from the combustion chamber (W)
$\lvert\dot{Q}'_{HC}\rvert$	heat rate transferred from the combustion chamber to the associated heat exchanger (W)
$\lvert\dot{Q}_{HS}\rvert$	heat rate input from the solar collector (W)
$\lvert\dot{Q}_{iHS}\rvert$	heat losses at the solar receiver (W)
$\lvert\dot{Q}'_{HS}\rvert$	heat rate transferred from the solar collector to the associated heat exchanger (W)
$\lvert\dot{Q}_l\rvert$	losses associated to heat transfers in the solar field (W)
$\lvert\dot{Q}_L\rvert$	heat-transfer rate between the working fluid and the ambient (W)
Q_{LHV}	lower heating value of the fuel (J/kg)
$\lvert\dot{Q}_{reh}\rvert$	heat rate input from the reheaters (W)
r_e	fuel conversion rate
r_p	overall pressure ratio
T_{HC}	working temperature of the combustion chamber (K)
T_{HS}	working temperature of the solar collector (K)
T_L	ambient temperature (K)
T_x	working fluid temperature after the heat input from the recuperator (K)
$T_{x'}$	working fluid temperature after heat input from the solar collector (K)
T_y	working fluid exhaust temperature (K)
T_1	compressors inlet temperature (K)
T_2	temperature after last compressor (K)
T_3	turbines inlet temperature (K)
T_4	temperature after last turbine (K)
$\overline{U}_L$	effective conduction–convection heat transfer coefficient [$W/(m^2 K)$]
α	effective emissivity
ε_{HC}	combustion chamber heat exchanger effectiveness
ε_{HS}	solar collector heat exchanger effectiveness
ε_L	cold side heat exchanger effectiveness
ε_c	isentropic efficiency of the compressors
ε_r	recuperator effectiveness
ε_t	isentropic efficiency of the turbines
γ	adiabatic coefficient of the working fluid
η	overall energy efficiency
η_c	combustion efficiency
η_h	thermal efficiency of the Brayton heat engine
η_s	solar collector efficiency
η_0	optical efficiency
ρ_H	irreversibilities due to pressure drops in the heat input
ρ_L	irreversibilities due to pressure drops in the heat release
σ	Stefan–Boltzmann constant ($W m^{-2} K^{-4}$)

predicted realistic values for efficiencies. Thus, sensitivity studies and optimization analyses can be done in more general terms than those done, for instance, with simulation software, as performed for instance by Barigozzi et al. [12,13]. Both techniques are complementary. Probably, general thermodynamic models are to be developed first in order to select adequate plant concepts and then detailed component-to-component simulations, are required to solve technical issues as done by Milani et al. [14] and to get to very detailed predictions of plant performance as shown in the work by Kalathakis et al. [15].

One of the main drawbacks of considering Brayton cycles in CSP applications is that for the compression stage much power is required, so the net power output becomes reduced. This point is detailed by Iverson et al. [16]. One possibility to avoid this handicap is to operate at supercritical conditions as suggested by Al-Sulaiman and Atif [17]. Extensive work has been devoted to this issue, specially considering carbon dioxide as working fluid, as done by Luu et al. [18]. Near the critical region fluids show numerical values for compressibility similar to liquids. Compression work can be reduced but as critical pressure for CO_2 is about 74 bar, high pressures have to be used. Vasquez et al. [19] point out that this leads to several technical problems. Moreover, wide fluctuations of thermodynamic properties near the critical point make difficult to develop thermodynamic models relying on ideal gas approximations. With respect to the turbomachinery much scarce experience has been acquired in components working with critical or transcritical fluids. A thorough review on this point is due to Ahn et al. [20]. An alternative way to reduce compression work is by joining these concepts: recuperation and multi-stage compression with intercooling. Recent works on these issues have been developed by Reyes-Belmonte et al. [21]. Additionally, if expansion is performed in several turbines with intermediate reheaters, temperature at the exit of the last turbine is high and so the potential for recuperation, as shown in the paper by Sánchez-Orgaz et al. [22].

Even though there is a great amount of works on the possibilities of using supercritical CO_2 in CSP systems, to our knowledge there are much scarce thermodynamical investigations on subcritical fluids as CO_2 together with multi-stage compression with intercooling and multi-stage expansion with reheating. Our work deals with this point. Plant configurations for central tower hybrid CSP plants working on closed atmospheric Brayton cycles for several working fluids shall be investigated, including subcritical CO_2, helium, nitrogen, and air. Plant performance will be compared by taking similar conditions for all fluids. Although the peculiarities of heat exchangers and turbomachinery of course rely on the type of fluid, components with similar effectivenesses or isentropic efficiencies will be assumed, *i.e.*, details on the design and performance of plant components are not analyzed, but it is assumed that with the appropriate design particularities components can have similar effectivenesses or isentropic efficiencies. To get that aim it is developed a thermodynamical model that incorporates the main irreversibilities existing in all the subsystems in these plants: solar, combustion chamber, and thermal engine. A simplified model was developed and validated in previous works by our group for the case of air and single-stage compression and expansion [23,24]. In this work it is extended for an arbitrary number of compression/expansion steps, recuperation, and for subcritical fluids by explicitly considering the temperature dependence of specific heats. Although the model allows for on-design and off-design analyses as shown in the study by Santos et al. [25], in this work design point parameters summarized by Quero et al. [26] from an experimental facility will be considered as reference case to compare with. The compression ratio is a key parameter in the design of any plant involving Brayton-like cycles. In our

study, first the results for different fluids at the same compression ratio will be compared and later specific values of the pressure ratio for each working fluid leading to maximum overall plant efficiency will be calculated.

In Section 2 the thermodynamic model and the main hypotheses assumed will be detailed. Explicit equations for heat transfers, subsystem efficiencies, and overall energy efficiency will be developed. Section 3 contains information about the considered reference plant, the design parameters, and the particularities of the elected working fluids. Numerical predictions on plant performance assuming the pressure ratio of the reference plant will be compared in Section 4 for different working gases. In Section 5 a numerical analysis to maximize plant performance in terms of the pressure ratio will be performed for each fluid. Section 6 is specifically devoted to plant configurations with two compression steps and intercooling. The plant performance for this kind of plant layouts will be compared for all the fluids considered.

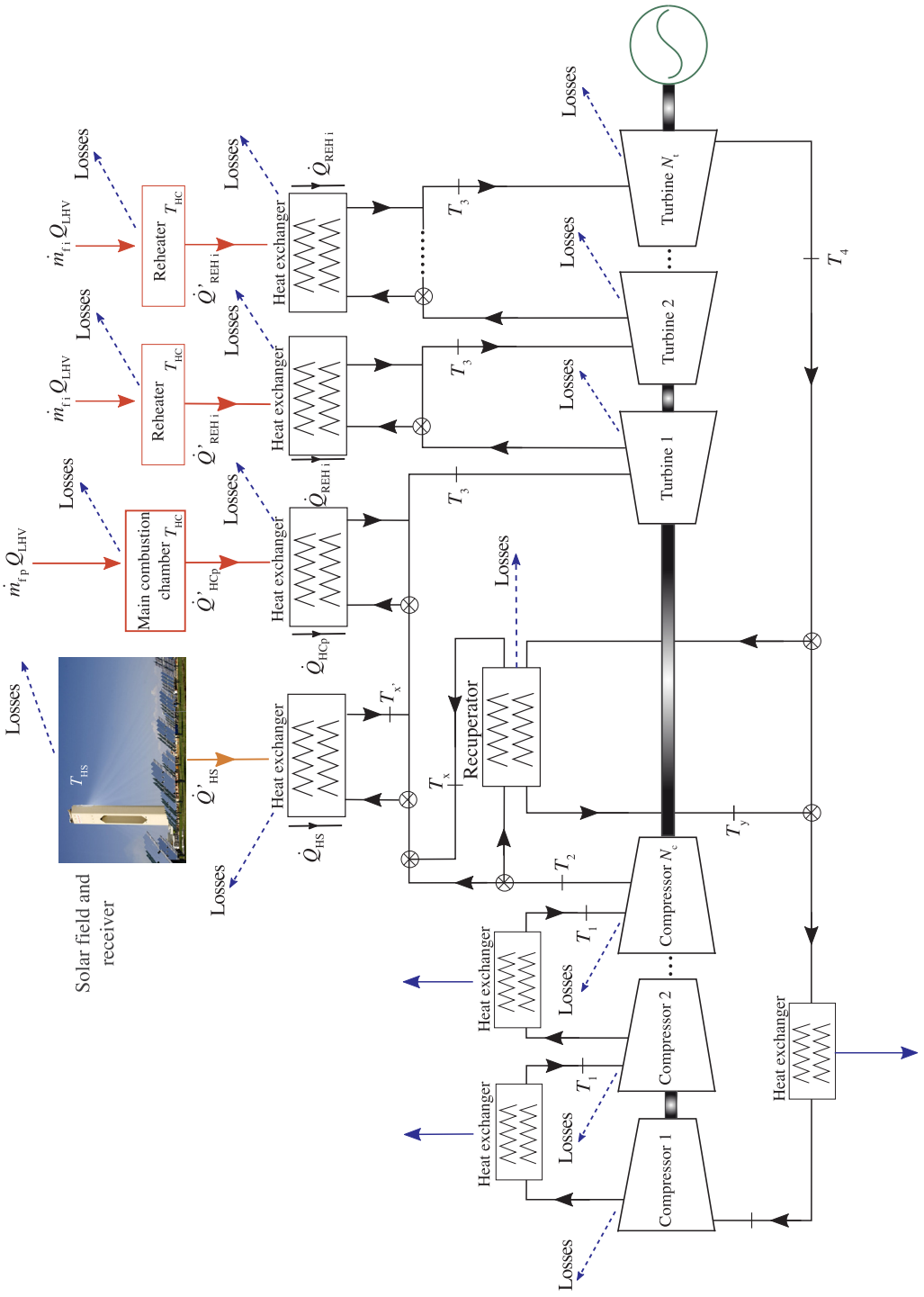

Fig. 1. Scheme of the hybrid solar gas-turbine plant considered. The plant includes a solar subsystem (solar field and central tower receiver), a main combustion chamber, an arbitrary number of compressors (N_c), and an arbitrary number of turbines (N_t). Between compressors N_c-1 intercoolers are considered and, similarly, between turbines N_t-1 intermediate reheaters. Losses in the thermodynamic model are shown in the picture. The ambient temperature, T_L, and the effective temperature of the solar receiver, T_{HS}, are fluctuating quantities, since depend on seasonal and meteorological conditions.

2. Plant thermodynamics

The considered system is a gas-turbine power plant hybridized with a central tower solar concentration system. An sketch of the whole system is depicted in Fig. 1. Briefly, the working fluid enters the first compressor at a temperature T_1, and exits the last one (N_c) at a temperature T_2. Between each pair of compressors, an intercooler is considered with the aim that the inlet temperature at each compressor is always T_1. After the last compressor the heat input in the power unit is divided in three subsequent steps:

1. A recuperator is used to take advantage of the residual heat after the last turbine. The fluid temperature at the recuperator exit is denoted as T_x.
2. When solar conditions are adequate, the fluid is redirected through the solar receiver and its temperature increases up to $T_{x'}$.
3. During night or poor insolation conditions the working fluid is conducted directly to the combustion subsystem. closed cycle is being considered, so the heat input from combustion is done through a heat exchanger associated to the main combustion chamber. Independently of solar conditions the combustion chamber ensures that the first turbine inlet temperature is stable, T_3.

The expansion stroke is performed by means of an arbitrary number of turbines, N_t. A number N_t-1 of intermediate reheaters make that for any turbine the inlet temperature is T_3. Afterwards the expansion process (temperature T_4) the fluid is redirected through the recuperator to another heat exchanger that ensures that the process is closed and cyclic, so the temperature at the compressor entrance in the following cycle is T_1. Fig. 2 contains a $T-S$ diagram of the thermodynamic cycle developed by the working fluid.

2.1. Heat fluxes, subsystem efficiencies, and overall efficiency

The overall plant energy efficiency, η, is defined as the fraction between the net mechanical power output, P, and the total heat input rate in the whole system. The latter is the sum of the heat input flows of the solar part and the combustion chamber:

$$\eta = \frac{P}{G A_a + \dot{m}_f Q_{\mathrm{LHV}}} \tag{1}$$

where G is the direct normal irradiance, A_a the aperture area of the heliostats field, Q_{LHV} the lower heating value of the fuel, and $\dot{m}_f$ is the sum of the fuel mass flows entering into the combustion chamber, $\dot{m}_{fp}$, as well as into the reheaters, $\dot{m}_{fi}$:

$$\dot{m}_f = \dot{m}_{fp} + \sum_{i=1}^{N_t-1} \dot{m}_{fi} \tag{2}$$

so, the overall efficiency is:

$$\eta = \frac{P}{G A_a + \left(\dot{m}_{fp} + \sum_{i=1}^{N_t-1} \dot{m}_{fi}\right) Q_{\mathrm{LHV}}} \tag{3}$$

Once expressed the efficiency in general terms, it will be rewritten as a function of the efficiencies of the subsystems that constitute the plant. The solar collector efficiency, η_s, is defined as the ratio between the useful energy per unit time provided by the collector, $|\dot{Q}'_{\mathrm{HS}}|$ (see Fig. 1), and the solar energy rate it receives, GA_a: $\eta_s = |\dot{Q}'_{\mathrm{HS}}|/GA_a$. The solar central tower transfers a fraction of the useful heat collected by the heliostats, $|\dot{Q}'_{\mathrm{HS}}|$, to the working fluid, that is denoted $|\dot{Q}_{\mathrm{HS}}|$. Introducing ε_{HS}, the effectiveness of the solar receiver (considered as a heat exchanger), $|\dot{Q}_{\mathrm{HS}}| = \varepsilon_{\mathrm{HS}}|\dot{Q}'_{\mathrm{HS}}|$, the solar collector efficiency can be expressed as: $\eta_s = |\dot{Q}_{\mathrm{HS}}|/(\varepsilon_{\mathrm{HS}} GA_a)$.

In a similar way the efficiency of the main combustion process, η_{cp}, is defined as the quotient between the heat flux from the combustion

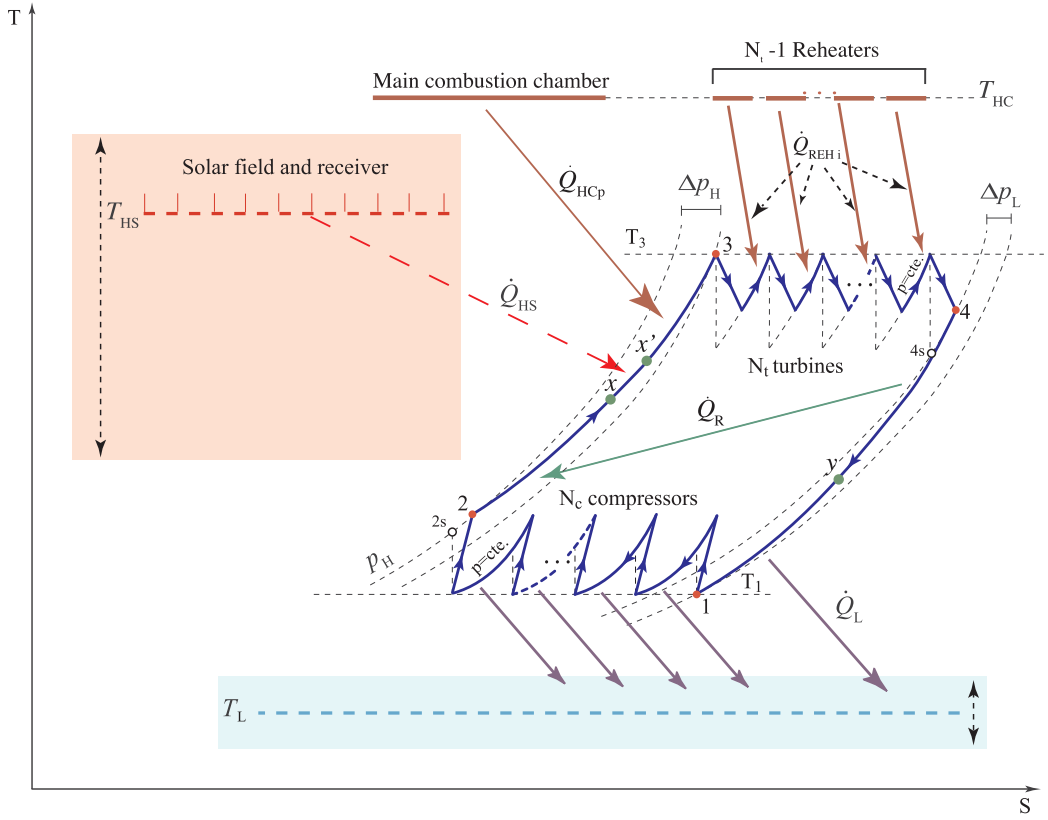

Fig. 2. Temperature-entropy diagram of the considered plant layout.

chamber and the energy contents of the entering fuel, $\dot{m}_f Q_{\mathrm{LHV}}$. The combustion chamber produces a heat rate, $|\dot{Q}'_{\mathrm{HCp}}|$, transferred to the working fluid through a heat exchanger whose effectiveness is $\varepsilon_{\mathrm{HCp}} = |\dot{Q}_{\mathrm{HCp}}|/|\dot{Q}'_{\mathrm{HCp}}|$, where $|\dot{Q}_{\mathrm{HCp}}|$ is the actual heat rate received by the working fluid from combustion. As a result, the combustion chamber efficiency can be written as:

$$\eta_{\mathrm{cp}} = \frac{|\dot{Q}_{\mathrm{HCp}}|}{\dot{m}_{fp}\,\varepsilon_{\mathrm{HCp}}\,Q_{\mathrm{LHV}}} \tag{4}$$

The combustion efficiency for each intermediate reheater, η_{ci}, is calculated alike:

$$\eta_{\mathrm{ci}} = \frac{|\dot{Q}_{\mathrm{rehi}}|}{\dot{m}_{fi}\,\varepsilon_{\mathrm{rehi}}\,Q_{\mathrm{LHV}}} \tag{5}$$

Each one has an associated heat exchanger with effectiveness, $\varepsilon_{rehi} = |\dot{Q}_{\mathrm{rehi}}|/|\dot{Q}'_{\mathrm{rehi}}|$.

The total heat input rate that the fluid absorbs from combustion is given as:

$$|\dot{Q}_{HC}| = |\dot{Q}_{HCp}| + |\dot{Q}_{reh}| \tag{6}$$

where

$$|\dot{Q}_{reh}| = \sum_{i=1}^{N_t-1} |\dot{Q}_{rehi}| \tag{7}$$

The efficiency of the thermal engine itself, η_h, is the ratio between the mechanical power output and the total heat input rate:

$$\eta_h = \frac{|\dot{W}|}{|\dot{Q}_H|} = \frac{P}{|\dot{Q}_{HS}| + |\dot{Q}_{HCp}| + |\dot{Q}_{reh}|} \tag{8}$$

Thus, the overall system efficiency, η, given by Eq. (1), is:

$$\eta = \frac{P}{\frac{|\dot{Q}_{HS}|}{\varepsilon_{HS}\,\eta_s} + \left[\frac{|\dot{Q}_{HCp}|}{\varepsilon_{HCp}\,\eta_{cp}} + \sum_{i=1}^{N_t-1}\frac{|\dot{Q}_{rehi}|}{\varepsilon_{rehi}\,\eta_{ci}}\right]} \tag{9}$$

Assuming identical efficiencies for the main combustion chamber and for reheaters, $\eta_{cp} = \eta_{ci} \equiv \eta_c$ and $\varepsilon_{HCp} = \varepsilon_{rehi} \equiv \varepsilon_{HC}$, the thermodynamic efficiency can be written as:

$$\eta = \frac{P}{\frac{|\dot{Q}_{HS}|}{\varepsilon_{HS}\,\eta_s} + \frac{|\dot{Q}_{HC}|}{\varepsilon_{HC}\,\eta_c}} = \eta_h\,\eta_s\,\eta_c\left(\frac{|\dot{Q}_{HS}| + |\dot{Q}_{HC}|}{\frac{\eta_c\,|\dot{Q}_{HS}|}{\varepsilon_{HS}} + \frac{\eta_s\,|\dot{Q}_{HC}|}{\varepsilon_{HC}}}\right) \tag{10}$$

It is interesting to define a solar share, f, as the ratio between the heat input rate from the sun and the total one:

$$f = \frac{|\dot{Q}_{HS}|}{|\dot{Q}_{HS}| + |\dot{Q}_{HC}|} \tag{11}$$

Depending on solar conditions, the solar share fluctuates in the interval [0,1]. $f = 1$, means that all the heat input has solar origin and $f = 0$ means that all the heat input comes from combustion, for instance by night. With this definition it is possible to express the overall plant efficiency in terms of the efficiency of the solar subsystem, η_s, that of the combustion chambers η_c, the efficiency of the Brayton heat engine η_h, the *solar share f*, and the effectivenesses of the heat exchangers between subsystems ε_{HS} and ε_{HC}:

$$\eta = \eta_h\,\eta_s\,\eta_c\left[\frac{1}{\frac{\eta_c f}{\varepsilon_{HS}} + \frac{\eta_s(1-f)}{\varepsilon_{HC}}}\right] = \eta_h\,\eta_s\,\eta_c\left[\frac{\varepsilon_{HS}\,\varepsilon_{HC}}{\eta_c f \varepsilon_{HC} + \eta_s(1-f)\varepsilon_{HS}}\right] \tag{12}$$

In the particular case of only solar heat input, $f = 1$, so $\eta = \eta_h\eta_s\varepsilon_{HS}$, and for only combustion $f = 0$, and $\eta = \eta_h\eta_c\varepsilon_{HC}$.

It is interesting to define an efficiency with an economic meaning, the *fuel conversion rate* as the ratio between the power output and the heat input rate with an associated cost, as proposed by Heywood [27]:

$$r_e = \frac{P}{\dot{m}_f\,Q_{LHV}} \tag{13}$$

It can be expressed in terms of the efficiency of the subsystems and the solar share as:

$$r_e = \frac{\eta\,\eta_s\,\eta_h\,\varepsilon_{HS}}{\eta_s\,\eta_h\,\varepsilon_{HS} - \eta f} \tag{14}$$

For pure solar operation ($\dot{m}_f = 0$), $f = 1$, and $r_e \to \infty$ and for only combustion operation, $f = 0$, so $r_e = \eta$.

2.2. Solar subsystem model

Next the model for the losses and efficiency for the solar subsystem is briefly summarized. An heliostat field with aperture area A_a and a central tower receiver with area A_r are considered. The solar power collected in the aperture is $|\dot{Q}_s| = GA_a$. Nevertheless, the energy flux collected at the tower is affected by optical losses associated to absorption by the heliostats, shadowing and blocking, spillage, ambient humidity, and others as stated by Collado and Turégano [28]. Details on these issues can be found in the work by López-Herráiz [29]. The most simple way to globally account for these effects is by defining an optical efficiency, η_0, so the heat input rate reaching the tower receiver is $|\dot{Q}_r| = \eta_0 GA_a$. Also there are heat transfer losses in the receiver due to convection, conduction and radiation. Heat losses can be expressed as (details can be found in the book by Duffie and Beckman [30] and the paper by Siva Reddy et al. [31]):

$$|\dot{Q}_l| = A_r\alpha\sigma(T_{HS}^4 - T_L^4) + A_r\overline{U_L}(T_{HS} - T_L) \tag{15}$$

where α is the emissivity of the receiver surface, $\overline{U_L}$ is an overall conduction and convection heat transfer coefficient, and σ the Stefan–Boltzmann constant. So, $|\dot{Q}'_{HS}| = |\dot{Q}_r - \dot{Q}_l|$, represents the effective heat flux that the receiver could transfer to the working fluid, assuming that it behaves as a heat exchanger. The energy rate finally absorbed by the working fluid considering the effectiveness of the receiver, ε_{HS} is:

$$|\dot{Q}_{HS}| = \varepsilon_{HS}\{\eta_0 GA_a - A_r[\alpha\sigma(T_{HS}^4 - T_L^4) + \overline{U_L}(T_{HS} - T_L)]\} \tag{16}$$

This energy rate, as depicted in Fig. 2 increases the working fluid temperature from T_x to $T_{x'}$ The efficiency of the solar subsystem, η_s, can be written as:

$$\eta_s = \eta_0[1 - h_1(T_{HS}^4 - T_L^4) - h_2(T_{HS} - T_L)] \tag{17}$$

where C is the concentration ratio, $C = A_a/A_r$ and h_1,h_2 are losses parameters, defined as: $h_1 = \alpha\sigma/(\eta_0 GC)$ and $h_2 = \overline{U_L}/(\eta_0 GC)$.

2.3. Combustion subsystem

The maximum energy that could be obtained from combustion is $\dot{m}_f Q_{LHV}$ considering ideal combustion and no losses in the combustion chamber. But actually the useful energy that can be transferred to the working fluid is only a fraction of that energy rate, $\eta_{cp}\dot{m}_f Q_{LHV}$. Moreover, as a closed cycle is being considered, the heat is transferred to the power unit through a heat exchanger associated to the combustion chamber with effectiveness, ε_{HCp}. Thus, the heat rate that is actually released to the working fluid can be written as: $|\dot{Q}_{HCp}| = \varepsilon_{HCp}|\dot{Q}'_{HCp}| = \varepsilon_{HCp}\,\eta_{cp}\,\dot{m}_{fp}\,Q_{LHV}$. In a similar way, for the intermediate reheaters:

$$|\dot{Q}_{reh}| = \sum_{i=1}^{N_t-1}\varepsilon_{rehi}|\dot{Q}'_{rehi}| = \sum_{i=1}^{N_t-1}\varepsilon_{rehi}\,\eta_{ci}\,\dot{m}_{fi}\,Q_{LHV} \tag{18}$$

Assuming that combustion efficiencies are the same for all the reheaters and equal to that of the main combustion and also that all the associated heat exchangers are similar:

$$|\dot{Q}_{reh}| = \varepsilon_{HC}\,\eta_c\,Q_{LHV}\sum_{i=1}^{N_t-1}\dot{m}_{fi} \tag{19}$$

Table 1
Thermodynamic properties of the considered working fluids: molecular weight (M), critical temperature and pressure (T_c and p_c respectively) and mean values of the constant pressure specific heat ($\bar{c}_w$) and adiabatic coefficient ($\bar{\gamma}$), in the temperature interval [288,1430] K. The coefficients of the fits of $c_w(T)$ [in units of J/(mol K)] correspond to the function: $c_w(T) = a + b\,T + c\,T^2 + d\,T^3 + e\,T^4$. Data for the fits were taken from [33] at a pressure $p = 5$ bar.

	He	N_2	Dry air	CO_2
M (g/mol)	4.00	28.01	28.97	44.01
T_c (K)	5.1953	126.19	132.84	304.13
p_c (bar)	2.2761	33.958	38.501	73.773
a	20.7862	32.3518	38.6449	25.4812
b	–	−0.02031	−0.044282	0.051549
c	–	4.2182×10^{-5}	7.9699×10^{-5}	-2.7778×10^{-5}
d	–	-2.7814×10^{-8}	-5.3556×10^{-8}	4.6551×10^{-9}
e	–	6.3098×10^{-12}	1.2726×10^{-11}	4.81185×10^{-13}
$\bar{\gamma}$	1.6667	1.3561	1.3458	1.1986
$\bar{c}_w$ [J/(g K)]	5.1965	1.1354	1.1202	1.1587

2.4. Multi-stage Brayton power unit model

In this section a model for the multi-stage Brayton cycle is proposed and its thermal efficiency, η_h, evaluated. The working fluid is considered as an ideal gas with temperature dependent specific heats, $c_w(T)$, following an irreversible recuperative Brayton cycle with multiple compression and expansion steps. The temperature-entropy diagram of the cycle is depicted in Fig. 2. In the following the main cycle stages are modeled together with the main irreversibility sources associated to each:

- In the first process (1 → 2), the working fluid is compressed through an arbitrary number, N_c, of compressors. They are considered identical, so the isentropic efficiency of any of them is: $\varepsilon_c = (T_{2s}-T_1)/(T_2-T_1)$, where T_{2s} would be temperature after compressions if they were isentropic (see Fig. 2). Between each pair of compressors, it is considered an intercooler, so the inlet temperature of all compressors is the same, T_1.
- Between states 2 and 3, three subsequent heat inputs increase the fluid temperature. First, a non-ideal recuperator increases temperature from T_2 up to T_x. Its effectiveness is defined as: $\varepsilon_r = (T_x-T_2)/(T_4-T_2) = (T_y-T_4)/(T_2-T_4)$. A non-recuperative plant is easily simulated by taking $\varepsilon_r = 0$. Second, if solar conditions are good enough, the fluid receives a solar heat input rate, $|\dot{Q}_{HS}|$, that rises up the temperature from T_x to $T_{x'}$. And third, the main combustion chamber provides the required energy to reach the turbines inlet temperature, T_3, that is assumed as a fixed input parameter. So, in principle (apart from fluctuations of the ambient temperature), the only oscillating temperature during heat input due to irradiance oscillations is $T_{x'}$. Although each subprocess during heat input has its own pressure losses, for simplicity a parameter that globally measures the whole pressure losses in the fluid during the heating process is assumed, $\rho_H = (p_H-\Delta p_H)/p_H$, where p_H is the highest pressure (compressor exit) and $p_H-\Delta p_H$ is the pressure at the first turbine inlet.
- At the state 3 the working fluid attains its maximum temperature and it is expanded by N_t subsequent gas turbines. Any of them is characterized by an isentropic efficiency $\varepsilon_t = (T_4-T_3)/(T_{4s}-T_3)$. To ensure that the temperature at any turbine inlet is T_3,N_t-1 intermediate reheaters are required. After the last turbine, the fluid reaches state 4.
- Finally, the fluid recovers the conditions of state 1 by means of a heat release that is split in two processes. The first associated to recuperation that ends at temperature T_y and the second through a heat exchanger that cools the fluid up to T_1. Its effectiveness is defined as: $\varepsilon_L = (T_1-T_y)/(T_L-T_y)$. The global pressure decay in 4 → 1 is measured by introducing a parameter: $\rho_L = (p_L-\Delta p_L)/p_L$ where p_L is the fluid pressure after the last turbine and $p_L-\Delta p_L$ the lowest pressure. It is convenient to define an overall pressure ratio as $r_p = p_H/(p_L-\Delta p_L)$.

Next, the objective is to obtain cycle temperatures and heat rates in terms of the parameters associated to cycle size and geometry, and thermal losses. By convenience, two parameters, a_c and a_t, related to pressure ratios of compressors and turbines are defined:

$$a_c = \frac{T_{2s}}{T_1} = \left(\frac{p_H}{p_L-\Delta p_L}\right)^{(\bar{\gamma}_{12}-1)/\bar{\gamma}_{12}} = r_p^{(\bar{\gamma}_{12}-1)/\bar{\gamma}_{12}} \tag{20}$$

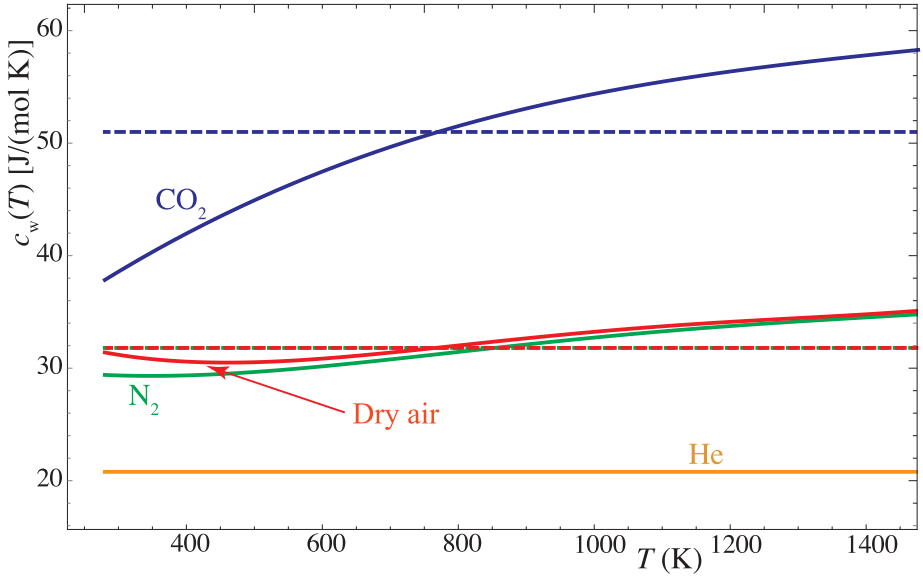

Fig. 3. Evolution with temperature of the constant pressure molar heats of the working fluids considered in the work. Average values are shown in dashed lines. Data were taken from [33] at a pressure $p = 5$ bar.

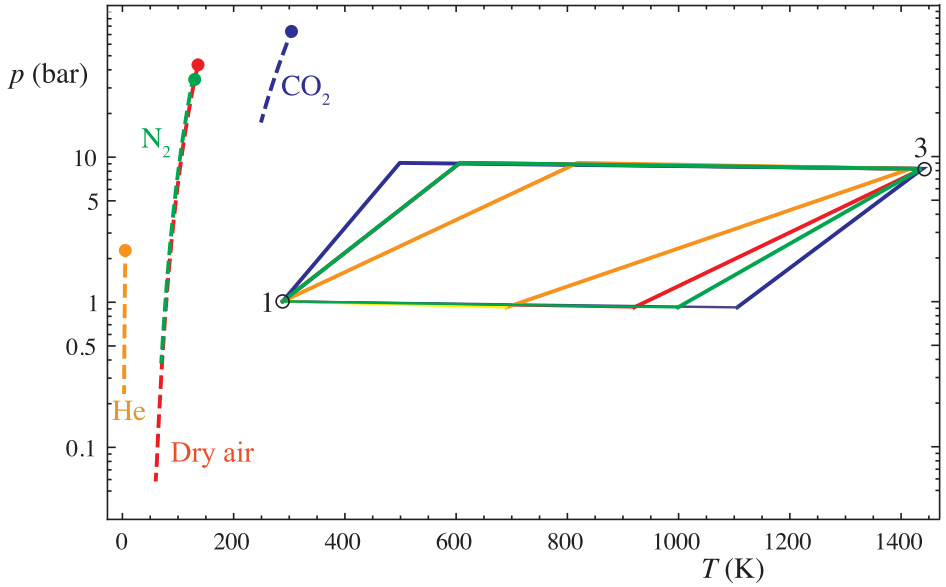

Fig. 4. $p-T$ approximate diagrams of the Brayton cycles followed by the considered working fluids. The vertical axis is represented in logarithmic scale. Dashed lines represent the liquid–vapor coexistence lines. Critical points for each fluid are shown as filled circles.

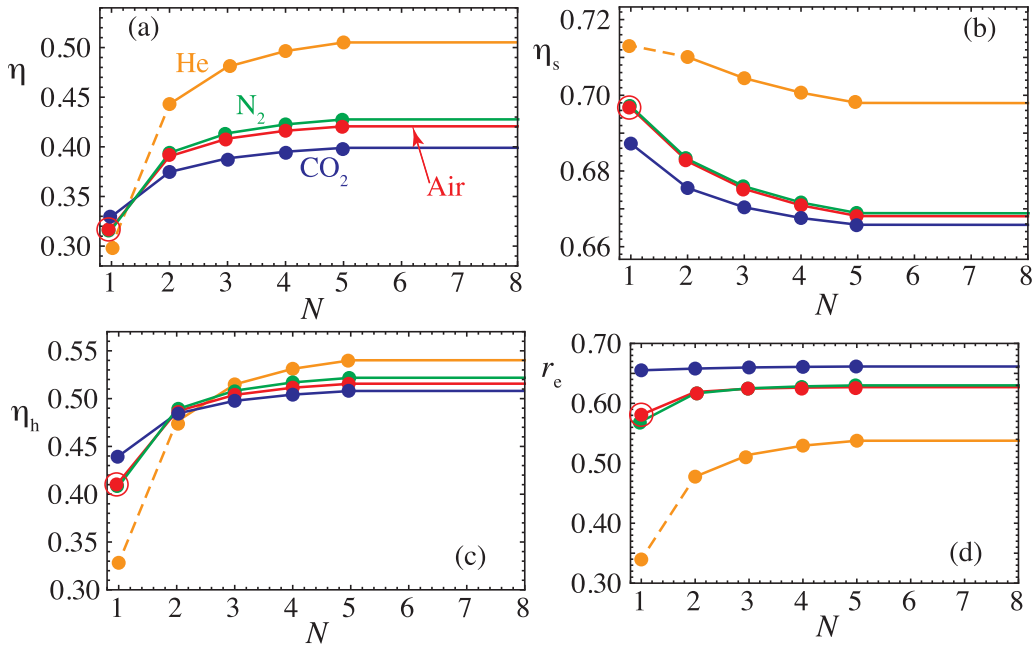

Fig. 5. Evolution of plant efficiencies (η, overall plant efficiency; η_s, solar subsystem efficiency; η_h, heat engine efficiency; and r_e, fuel conversion rate) with the number of compression/expansion stages assumed identical, $N_t = N_c \equiv N$, for all the fluids considered. The reference values corresponding to the Solugas project are marked with an open circle. Lines between points are just a guide for the eye. Lines are dashed for He between N = 1 and the other cases because for N = 1 no regeneration is considered. The input data are those in Section 3.

Table 2
Percentage relative variations of the estimated efficiencies with respect to the reference values of the Solugas project (points marked with an open circle in Fig. 5). In the case of He and N = 1, no regeneration is considered (NR). The pressure ratio was taken in all cases as in the gas turbine of the Solugas project, $r_p = 9.9$. The case of a large number of compression/expansion stages is represented as $N \to \infty$.

Working fluid	Dry Air		N_2			He			CO_2		
N	2	$N \to \infty$	1	2	$N \to \infty$	$1^{(NR)}$	2	$N \to \infty$	1	2	$N \to \infty$
η	22.623	36.956	−0.560	23.713	39.868	−5.894	39.132	67.745	3.577	17.656	29.970
η_h	17.967	28.476	−0.985	18.489	30.611	−20.427	15.373	38.138	6.655	17.388	26.674
η_s	−2.026	−6.030	0.0593	−1.941	−5.894	2.359	1.932	−1.986	−1.352	−3.037	−5.563
r_e	6.531	8.119	−1.921	6.139	9.180	−41.557	−17.778	−2.833	12.768	13.262	14.245

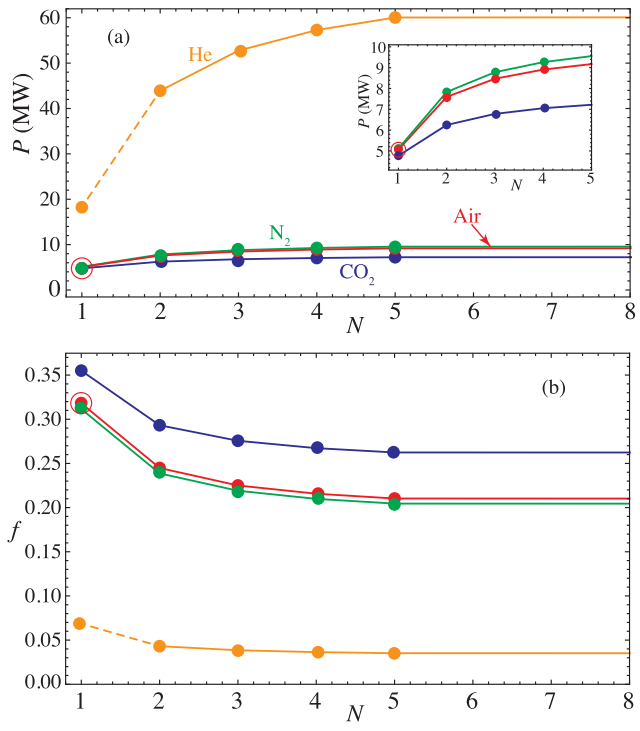

Fig. 6. Evolution of the power output, P, and the solar share, f, with N. Open circles show the values corresponding to the reference Solugas plant. The inset shows a zoom with the behavior of air, N_2, and CO_2 with changing values of N.

$$a_t = \frac{T_3}{T_{4s}} = \left(\frac{p_H - \Delta p_H}{p_L}\right)^{(\overline{\gamma}_{34}-1)/\overline{\gamma}_{34}} \tag{21}$$

In these definitions it was considered that processes $1 \rightarrow 2s$ and $3 \rightarrow 4s$ are isentropic. $\overline{\gamma}_{12}$ is the mean value of the adiabatic constant in the temperature interval $[T_1, T_2]$ and similarly for $\overline{\gamma}_{34}$. Those temperature intervals are not large, so it is reasonable to work on average values

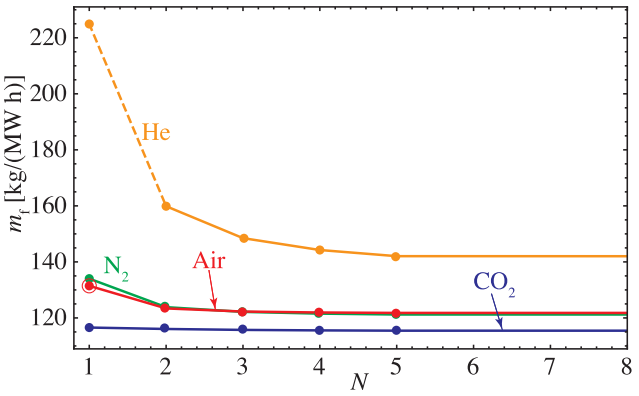

Fig. 8. Specific fuel consumption as a function of N. The open circle shows the value corresponding to the reference Solugas plant.

instead of temperature dependent parameters. From the definitions of ρ_H and ρ_L it is easy to show that the overall pressure ratio, r_p, and a_t are related by:

$$a_t = (\rho_H \rho_L r_p)^{(\overline{\gamma}_{34}-1)/\overline{\gamma}_{34}} \tag{22}$$

Thus, considering all the assumptions and definitions explained before, it is possible (after some algebraic calculations) to obtain analytical expressions for all cycle temperatures:

$$T_1 = \varepsilon_L T_L + T_y(1-\varepsilon_L) \tag{23}$$

$$T_2 = T_1 + \frac{1}{\varepsilon_c}(T_{2s} - T_1) = T_1 Z_c \tag{24}$$

$$T_3 = \varepsilon_{HC} T_{HC} + T_{x'}(1-\varepsilon_{HC}) \tag{25}$$

$$T_4 = T_3 - \varepsilon_t (T_3 - T_{4s}) = T_3 Z_t \tag{26}$$

$$T_x = \varepsilon_r T_4 + T_2(1-\varepsilon_r) \tag{27}$$

$$T_y = \varepsilon_r T_2 + T_4(1-\varepsilon_r) \tag{28}$$

$$T_{x'} = \varepsilon_{HS} T_{HS} + T_x(1-\varepsilon_{HS}) \tag{29}$$

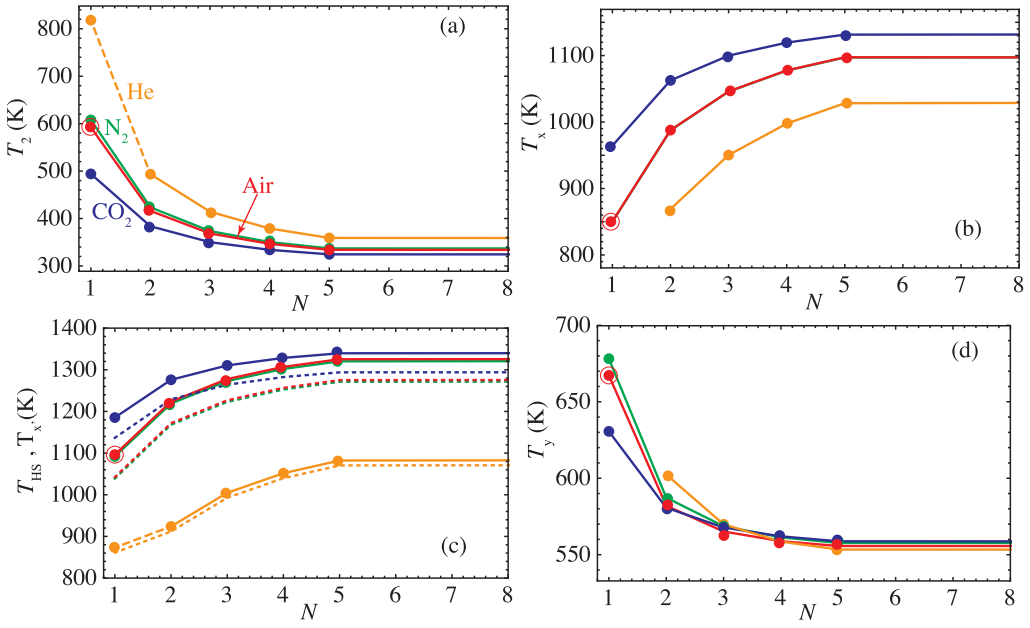

Fig. 7. Sensitivity of some plant temperatures to N: (a) T_2, compressors outlet temperature; (b) T_x, fluid temperature after regeneration; (c) T_{HS}, solar collector working temperature and $T_{x'}$, temperature of the fluid after absorbing the solar heat (shown in dotted lines in the bottom left plot); and (d) T_y, gas temperature at the output of the regeneration hot stream. Open circles show the values corresponding to the reference Solugas plant. In the case of He and N = 1 no regeneration is considered so the corresponding points for T_x and T_y does not appear in the plots.

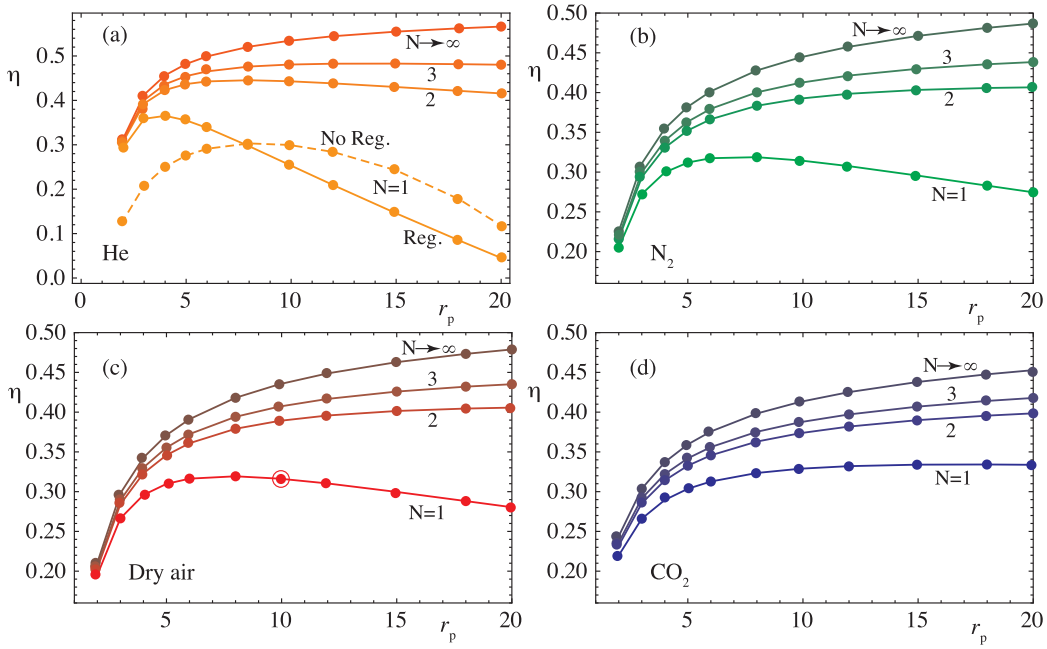

Fig. 9. Overall plant efficiency plotted against the pressure ratio for the considered working fluids: (a) He, (b) N_2, (c) air, and (d) CO_2. Several multi-step configurations are considered. In the case of He and $N = 1$ (top left figure) regenerative (solid line) and non-regenerative plant configurations are plotted (dashed line). The reference efficiency of the Solugas plant is shown for air as an open circle.

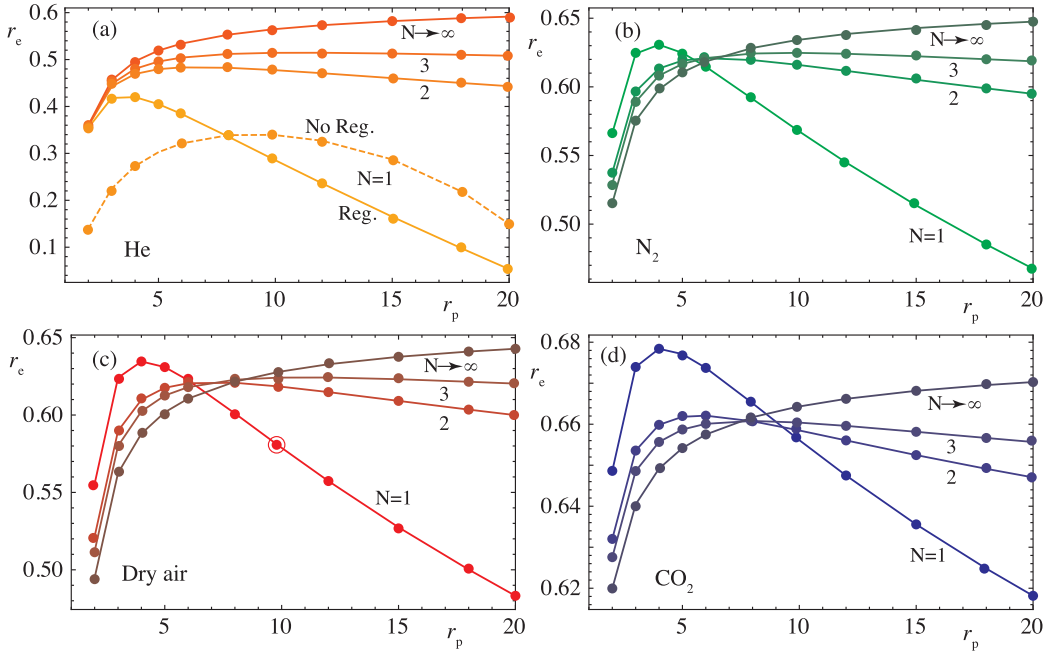

Fig. 10. Fuel conversion rate, r_e, against the pressure ratio, r_p for the considered working fluids: (a) He, (b) N_2, (c) air, and (d) CO_2. In the case of He and $N = 1$ (top left figure) regenerative (solid line) and non-regenerative plant configurations are plotted (dashed line).

where other two definitions were included:

$$Z_c = 1 + \frac{1}{\varepsilon_c}\left(a_c^{1/N_c} - 1\right) \tag{30}$$

$$Z_t = 1 - \varepsilon_t\left(1 - \frac{1}{a_t^{1/N_t}}\right) \tag{31}$$

By using all these equations, temperatures T_2 and T_4 can be written as functions of the temperatures of the heat sources, T_{HS} and T_{HC}, the ambient temperature, T_L, the overall pressure ratio, r_p and the irreversibility parameters. This leads to:

$$\frac{T_2}{} = \frac{(1-\varepsilon_L)(1-\varepsilon_r)[\varepsilon_{HC}T_{HC} + \varepsilon_{HS}T_{HS}(1-\varepsilon_{HC})] + \varepsilon_L T_L[Z_t^{-1} - (1-\varepsilon_{HC})(1-\varepsilon_{HS})\varepsilon_r]}{[Z_c^{-1} - (1-\varepsilon_L)\varepsilon_r][Z_t^{-1} - (1-\varepsilon_{HC})(1-\varepsilon_{HS})\varepsilon_r] - (1-\varepsilon_{HC})(1-\varepsilon_{HS})(1-\varepsilon_L)(1-\varepsilon_r)^2} \tag{32}$$

$$\frac{T_4}{} = \frac{[\varepsilon_{HC}T_{HC} + \varepsilon_{HS}T_{HS}(1-\varepsilon_{HC})][Z_c^{-1} - (1-\varepsilon_L)\varepsilon_r] + \varepsilon_L T_L(1-\varepsilon_{HC})(1-\varepsilon_{HS})(1-\varepsilon_r)}{[Z_c^{-1} - (1-\varepsilon_L)\varepsilon_r][Z_t^{-1} - (1-\varepsilon_{HC})(1-\varepsilon_{HS})\varepsilon_r] - (1-\varepsilon_{HC})(1-\varepsilon_{HS})(1-\varepsilon_L)(1-\varepsilon_r)^2} \tag{33}$$

Any other temperature can be obtained in the same terms by

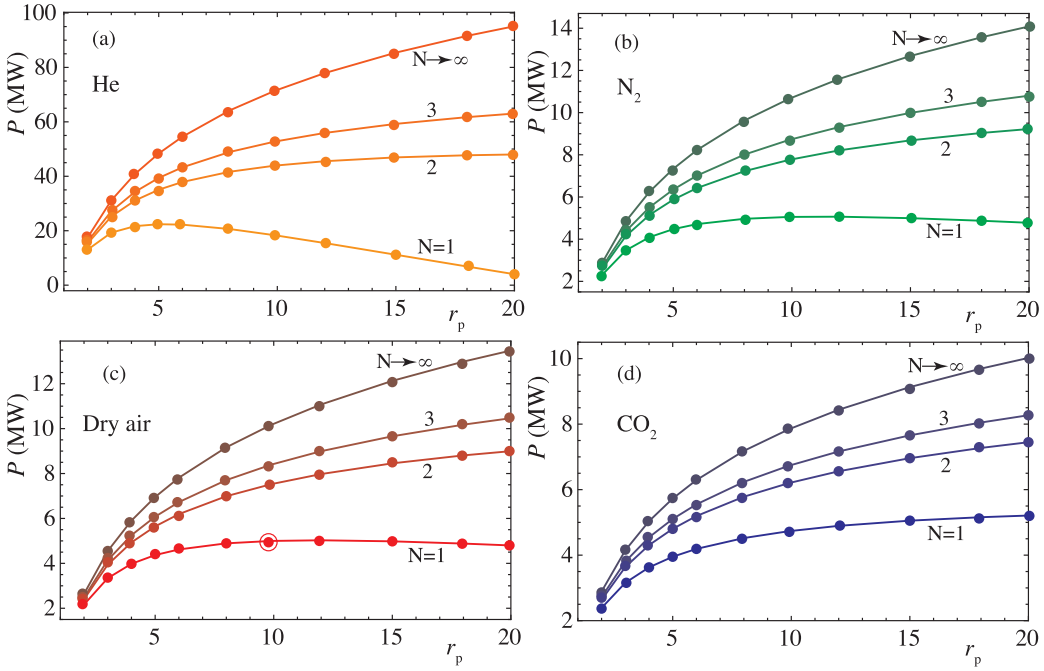

Fig. 11. Power output, P, against the pressure ratio, r_p for the considered working fluids: (a) He, (b) N_2, (c) air, and (d) CO_2.

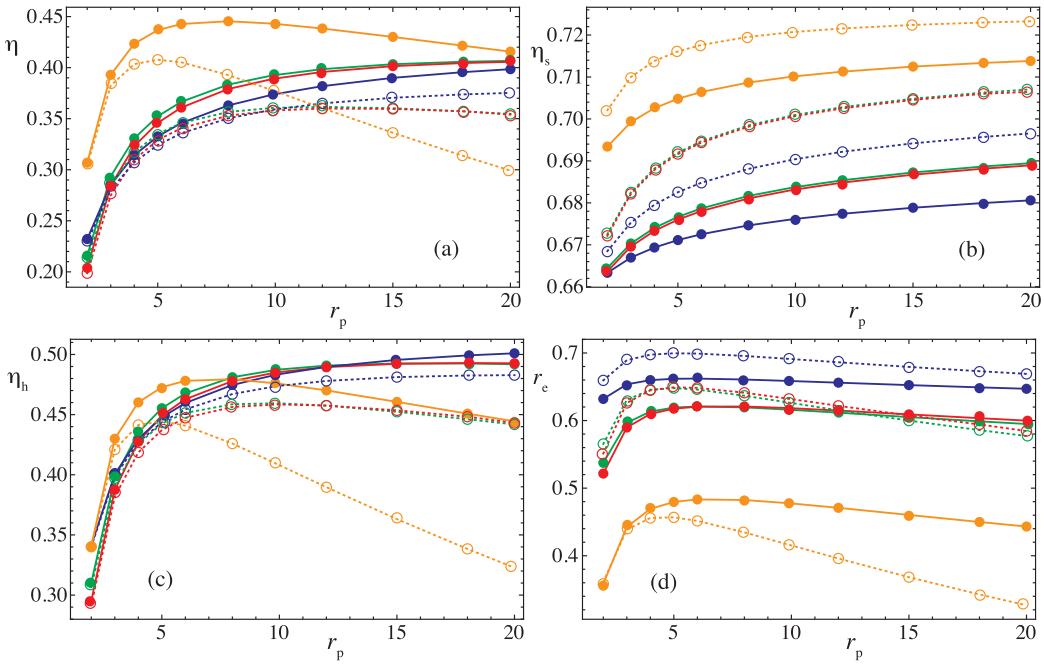

Fig. 12. Plant efficiencies as functions of the pressure ratio for different working fluids (helium, orange; dry air, red; nitrogen, green, and carbon dioxide, blue) and two particular configurations: $N_t = N_c = 2$ (solid lines) and $N_t = 1; N_c = 2$ (dashed). (For interpretation of the references to colour in this figure legend, the reader is referred to the web version of this article.)

substituting Eqs. (32) and (33) in Eqs. (23)–(29).

Now it is feasible to calculate all the components of the heat input rate, $|\dot{Q}_H| = |\dot{Q}_{HS}| + |\dot{Q}_{HCp}| + |\dot{Q}_{reh}|$, by using temperature equations and Eqs. (6) and (7):

$$|\dot{Q}_{\mathrm{HS}}| = \dot{m} \int_{T_x}^{T_{x'}} c_w(T)\,dT = f|\dot{Q}_H| \tag{34}$$

$$|\dot{Q}_{\mathrm{HCp}}| = \dot{m} \int_{T_{x'}}^{T_3} c_w(T)\,dT \tag{35}$$

$$|\dot{Q}_{reh}| = \dot{m} \sum_{j=1}^{N_t-1} \int_{T_j}^{T_3} c_w(T)\,dT \tag{36}$$

where T_j is the temperature at the exit of turbine j. In order to obtain an analytical expression for the last equation it will be assumed that the difference between T_3 and the temperatures at turbines exit, T_j, is not large, so a mean value for $c_w(T)$,$\bar{c}_{w,34}$ is considered. This hypothesis allows to write:

Table 3
Maximum values of overall efficiency (η_{max}), fuel conversion efficiency ($r_{e,max}$), maximum power output (P_{max}), and minimum specific fuel consumption ($m_{f,min}$). The corresponding pressure ratios, r_p, for cycles with $N_c = N_t = 2$ and $N_c = 2, N_t = 1$ are also shown. The reference values of the Solugas project, denoted as (Ref.), are included for comparison.

	η_{max}	r_p	$r_{e,max}$	r_p	P_{max} (MW)	r_p	$m_{f,min}$ [kg/(MW h)]	r_p
Ref.	0.32	9.9	0.58	9.9	5.06	9.9	132	9.9
				$N_c = N_t = 2$				
Dry air	0.41	20	0.62	6	9.0	20	121	6
N_2	0.41	20	0.62	6	9.2	20	121	6
He	0.45	8	0.48	6	48.0	20	158	6
CO_2	0.40	20	0.66	6	7.4	20	118	6
				$N_c = 2, N_t = 1$				
Dry air	0.36	12	0.65	5	6.4	20	118	5
N_2	0.37	12	0.65	5	6.6	20	118	5
He	0.41	5	0.45	5	29.3	8	170	5
CO_2	0.38	20	0.70	5	6.1	20	108	5

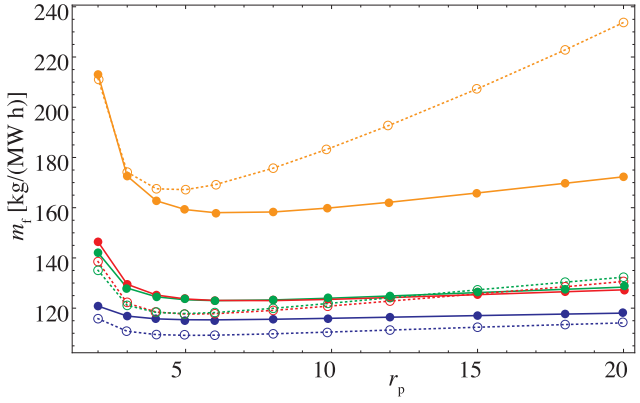

Fig. 13. Specific fuel consumption in terms of the pressure ratio for different working fluids (helium, orange; dry air, red; nitrogen, green, and carbon dioxide, blue) and two particular configurations: $N_t = N_c = 2$ (solid lines) and $N_t = 1; N_c = 2$ (dashed). (For interpretation of the references to colour in this figure legend, the reader is referred to the web version of this article.)

$$|\dot{Q}_{reh}| = \dot{m} \sum_{j=1}^{N_t-1} \int_{T_{js}}^{T_3} c_w(T)\,dT \simeq \dot{m}\,\varepsilon_t\,\bar{c}_{w,34} \sum_{j=1}^{N_t-1} (T_3 - T_{js}) = \dot{m}\,\bar{c}_{w,34}\,\varepsilon_t\,(N_t-1)(1-a_t^{-1/N_t})\,T_3 \tag{37}$$

The heat released by the working fluid to the cold source in the closed cycle can be expressed as:

$$|\dot{Q}_L| = \dot{m} \int_{T_1}^{T_y} c_w(T)\,dT + \dot{m} \sum_{k=1}^{N_c-1} \int_{T_1}^{T_k} c_w(T)\,dT \tag{38}$$

Assuming that the difference between T_1 and the temperature at any compressor exit is not large, a mean value of the specific heat, $\bar{c}_{w,12}$, is taken in order to calculate the total heat release rate:

$$|\dot{Q}_L| = \dot{m} \int_{T_1}^{T_y} c_w(T)\,dT + \dot{m} \frac{\bar{c}_{w,12}}{\varepsilon_c} \sum_{s=1}^{N_c-1} (T_{ks} - T_1) \tag{39}$$

The second term at the right side can be calculated as:

$$\dot{m} \frac{\bar{c}_{w,12}}{\varepsilon_c} \sum_{s=1}^{N_c-1} (T_{ks} - T_1) = \dot{m} \frac{\bar{c}_{w,12}}{\varepsilon_c} (N_c-1)(a_c^{1/N_c}-1)\,T_1 \tag{40}$$

and finally,

$$|\dot{Q}_L| = \dot{m} \int_{T_1}^{T_y} c_w(T)\,dT + \dot{m} \frac{\bar{c}_{w,12}}{\varepsilon_c} (N_c-1)(a_c^{1/N_c}-1)\,T_1 \tag{41}$$

The power output provided by the plant is then calculated as:

$$P = |\dot{Q}_H| - |\dot{Q}_L| \tag{42}$$

and its thermal efficiency through:

$$\eta_h = \frac{P}{|\dot{Q}_H|} \tag{43}$$

Before finishing this section it is convenient to recall that from the assumed plant scheme (see Fig. 2), the following conditions for the temperatures at the hot side hold:

$$T_3 \geqslant T_{x'} \geqslant T_x \tag{44}$$

$$T_{HS} \geqslant T_x \tag{45}$$

$$T_{HC} \geqslant T_{x'} \tag{46}$$

Also, in summary, its worth to note that with respect to the dependence of specific heats with temperature it was assumed that temperature changes in compression ($1 \rightarrow 2$) and expansion ($3 \rightarrow 4$) processes are small so mean values were taken ($\bar{c}_{w,12}$ and $\bar{c}_{w,34}$, respectively). Nevertheless, during heat input and release, of course changes could be large so explicit polynomials for $c_w(T)$ will be taken. These assumptions allow to obtain straightforward analytical expressions for all the temperatures in the cycle and so, to analyze the sensitivity of the performance of the whole plant to any design or irreversibility parameter. Accounted irreversibilities for the thermodynamic engine are external (arising from the coupling of the heat engine to the external heat sources, ε_{HS} and ε_{HC}) and internal (associated to compressors, ε_c, turbines, ε_t, recuperator, ε_t, and pressure losses, ρ_H and ρ_L).

3. Numerical computations

In this section details about the numerical implementation of the model previously developed will be presented. Particularly, the data concerning the plant sizing and operation, model validation, and particularities of the considered working fluids are exposed.

3.1. Design point conditions and model validation

The thermodynamic model presented in this work in the particular case of single-stage compression and expansion was applied in previous works by our group in order to predict the performance records of a project developed by *Abengoa Solar* near Seville, Spain, called *Solugas Project* [7]. In this project a natural gas commercial single-stage gas turbine (*Caterpillar Mercury 50*) was modified in order to be hybridized with a central tower solar receiver [26].

First, the model was validated for the turbine working at full load on an only combustion mode. This turbine operates at a pressure ratio $r_p = 9.9$ with an air gas flow $\dot{m} = 17.9$ kg/s. The turbine inlet temperature is $T_3 = 1423$ K and provides 4.6 MWe fueled with natural gas [25]. The manufacturer reports a thermal efficiency after generator, $\eta_{h,e} = 0.385$ for $T_L = 288$ K [32]. Our model is capable to reproduce the thermal efficiency of the turbine with a deviation below 0.5% and the power output below 1.5%. The following parameters were assumed in the model: $\varepsilon_{HC} = 0.98, \varepsilon_{HS} = 0.78, \varepsilon_L = 1, \rho_H = \rho_L = 0.97$ (relative global pressure losses about 9.2%), $\varepsilon_c = 0.885, \varepsilon_t = 0.815$, and $\varepsilon_r = 0.775$. Details on the calculations and explicit tables with the parameters can be found in a previous work by Santos et al. [25].

The plant developed for the Solugas project was also simulated operating in hybrid conditions at design point solar irradiance ($G = 860$ W/m^2) and ambient temperature ($T_L = 288$ K). The parameters considered for the solar subsystem are: $\eta_0 = 0.73, \alpha = 0.1, \varepsilon_{HS} = 0.95, C = 425.2$, and $\overline{U_L} = 5$ W/(m^2 K). In these conditions the model (considering dry air with temperature dependent specific heat) predicts an overall plant efficiency, $\eta = 0.32$, a fuel conversion efficiency, $r_e = 0.58$, a solar share $f = 0.32$, a specific fuel

consumption, $m_f = 132$ kg/(MWh), and a mechanical power output $P = 5.06$ MW. The objective of this work is focused on the analysis of the model predictions if the single-stage gas turbine was substituted by a multi-step one, and also on the influence of other possible working fluids, different from air. In the next subsection the interest of using different working fluids in the search for improved plant performance is motivated. The basic parameters of the Solugas plant will be assumed as reference values.

3.2. Working fluids

The advantages of closed gas turbines when compared with either those working on open cycle or when compared with Rankine cycles are diverse (a recent comprehensive review is due to Olumayegun et al. [4]): closed-cycle gas turbines at high temperatures can reach efficiencies similar to steam cycles, lead to simpler plant designs (less number of heat exchangers, pumps, and piping), and have more compact components and so lower size for a fixed rated power output. Moreover, unlike open-cycle Brayton plants can use dirty fuels as biomass and other heat sources (nuclear and solar for instance). And moreover, different working fluids (depending on their thermal and transport properties, and practical issues) can be used, as analyzed by Najjar and Zaamout [34]. This work is focused on the last point.

As mentioned by Olumayegun et al. [4], among the working fluids that have been used in closed-cycle prototype or real installations, the most usual are: air, nitrogen, helium, carbon dioxide, other noble gases as argon and neon, and also gas mixtures. The experience on the design and operation of closed-cycle turbines working with air is broad. This constitutes an evident advantage. On the contrary, these plants have considerable pressure losses, require high turbine inlet temperatures that contribute to materials oxidization, and air has a low heat transfer coefficient. For nitrogen considerations are similar because the experience from air turbines can be applied and most properties are alike. One difference with air is the behavior of materials at high temperatures that in this case nitrides instead of oxidizes.

The use of helium is related with the development of nuclear reactors. No et al. [35] give a detailed historical review of several facilities of this type. Helium is inert and non-toxic, has a good heat transfer coefficient, and low pressure losses. As drawbacks it should be highlighted that turbomachinery design experience is not so broad as for air, requires high turbine inlet temperature, leakage is high, and actually more number of turbomachinery stages are required, as analyzed by McDonald [36].

Carbon dioxide has been used as working fluid for closed Brayton cycle plants from 1950, mainly partially condensed or supercritical. From late 1990s and early 2000s there have been a renewed interest because research and development work has rapidly evolved turbomachinery and heat exchangers. A recent review has been published by Crespi et al. [37]. Solar applications are being also investigated and analyzed nowadays (see for instance the work by Coco-Enríquez et al. [38]. CO_2 is non-toxic and inert, has a favorable critical point and in supercritical conditions turbomachinery is small and compact and gives good efficiencies at moderate turbine temperatures. Similarly to helium, design experience is not wide, as pointed out by Chacartegui et al. [39]. Moreover, thermodynamic properties vary considerably in the vicinity of the critical point, so detailed investigation on compressors, turbines and other machinery is required. Nevertheless, works on subcritical CO_2 with solar applications are scarce. It is worth mentioning the work by Najjar et al. [34].

In our study four working fluids are considered: air, nitrogen, helium, and carbon dioxide. Table 1 contains several thermodynamic properties relevant to the application of our model as critical point conditions and evolution with temperature of molar heat, that is plotted in Fig. 3. The figure shows that carbon dioxide has a molar heat about twice larger that a monoatomic gas like He and that its dependence with temperature in the interval from ambient temperature to the temperature at turbine inlet is large. The curves for air and N_2 are in between those for CO_2 and He. The dependence of their $c_w(T)$ with temperature is not large in the operation interval.

Fig. 4 displays a $p-T$ diagram with the liquid–vapor coexistence curve and the approximate processes experienced by the fluids in the Brayton cycle (in the single-stage case). It was assumed atmospheric pressure at compressor inlet and a pressure ratio of 9.9 as in the Solugas project. Within these hypotheses, the considered gases are in subcritical conditions except for He, that performs a transcritical cycle because pressure of states 2 and 3 are above the critical pressure. The aim of our work is to analyze the influence of the working fluid on the performance of the plant from a purely thermodynamic model. It is noteworthy to mention that technical issues related to piping and turbomachinery design are not considered in detail. Relative pressure drops in the cycle and isentropic efficiencies for compressors and turbines are assumed to be alike for all fluids. Similarly, the same inlet pressure at the compressor and the same working fluid mass flow are supposed. Although from a technical viewpoint an exhaustive study of the mentioned issues would be imperative, the objective of this work is to investigate the role played by the thermodynamic properties of the fluids, specially the influence of the molar heat, $c_w(T)$, in the heat absorption and heat release processes. In consequence conclusions about the influence of the working fluid on plant output records, for different plant layouts in terms of the number of compression/expansion processes at similar conditions, can be extracted.

4. Numerical predictions on plant performance

Model predictions within the considerations detailed in the previous section are presented hereafter. Most significant plant efficiencies are plotted in Fig. 5 in terms of the number of compression, N_c, and expansion steps, N_t, assumed identical: $N_t = N_c = N$. In all the plots the reference values corresponding to the Solugas project (air as working fluid and $N = 1$) are marked with an open circle. Table 2 displays the relative increments with respect to that case. For instance, in the case of air, when considering two compressors with intercooling and two turbines with reheating ($N = 2$), the overall plant efficiency, η, experiences an increase about 23% with respect to $N = 1$. The addition of more compression/expansion stages could increase overall efficiency up to 37% approximately.

The evolution of the global efficiency curves for all fluids are similar: a rapid increase from $N = 1$ to $N = 2$ or 3 and a subsequent slower increase up to an asymptotic value. This evolution for the overall efficiency, η (Fig. 5(a)), comes essentially from that of the Brayton heat engine, η_h, displayed in Fig. 5(b). The behavior of air and nitrogen is similar, although the curve for nitrogen is slightly above. On the contrary, CO_2 shows values for η larger than those for air or nitrogen for $N = 1$, but the increase with the number of compression/expansion stages is slower. The case of He is different. First,for N = 1 no regeneration was considered. This is because for the considered pressure ratio (assumed for all the fluids at the design point of Solugas project) is too high for regeneration to be advantageous (see the graph corresponding to He in Fig. 4). This point will be analyzed below, when presenting the plots for cycle temperatures. And second, the overall efficiencies for $N \geqslant 2$ are quite above those for air or nitrogen. For instance, for $N = 2$,η increases about 39% with respect to the reference case for He and 23% for air or nitrogen. This larger values of η for He are essentially associated to the values of the solar subsystem efficiency, η_s (Fig. 5(c)), that are larger for He (this point will be resumed when presenting the results for temperatures). The values of η_h for helium are above those for air but only slightly for $N \geqslant 3$.

The evolution of solar subsystem efficiencies, η_s (Fig. 5(b)), with N displays a monotonic decreasing behavior because the operating temperatures of the solar collector increases with N and so losses become larger. Anyway, the interval of numerical values in which η_s evolves is quite narrow (see the vertical axis in the plot for η_s). The behavior of the

fuel conversion rate, r_e (the ratio between the power output and the heat input with an economic cost), is quite diverse and interesting (Fig. 5(d)). r_e is larger for CO_2 that for the other fluids, and almost independent of N. These values are about 13% over that for the reference case (see Table 2). Nevertheless, for air, N_2 and He, r_e increases with N. The poorest values of r_e are those for helium.

The power output is much larger for He that for the other fluids as displayed in Fig. 6(a). This is an effect associated to the conditions in which the results for the different fluids are being compared. The numerical magnitude of power output is proportional to $\dot{m}c_w$. Helium has a constant pressure specific heat, c_w, about 4 times larger than the other fluids (see the mean values in Table 1). As the working fluid mass flow is assumed to be the same for all fluids, power output for He is for $N = 1$ larger than for the rest of considered fluids in the same proportion that c_w. This effect is amplified for larger values of N due to the heat input in the reheaters between turbines. For the other fluids power output increases with N up to approximately $N = 3$. For larger N power output remains almost constant. The increase is larger for air and nitrogen. The inset in the figure shows that for $N \geqslant 2$ expected power output is larger for N_2 than for air.

The solar share, f (Fig. 6(b)), decreases for all fluids with the number of compression/expansion stages. This is associated to the increase of heat input from combustion in the intermediate reheaters between turbines. Largest solar share is observed for CO_2 and $N = 1$, where $f \simeq 0.35$. On the other side, solar heat input for helium is always very small. The solar subsystem size (aperture area) in the reference plant would be undersized for He and in consequence, the fuel conversion efficiency, r_e, is low.

Several cycle temperatures are depicted in Fig. 7. The temperature at the compressors exit, T_2 (Fig. 7(a)) decreases with N and reaches very high values for He, especially for $N = 1$. This is the reason why regeneration in this case (for the considered value of the pressure ratio, $r_p = 9.9$) is meaningless. For all the fluids, as N increases, the values of T_2 decrease, because intercooling between compressors makes the temperature decrease before the fluid enters the following compressor. The effective temperature of the solar collector, T_{HS} and the temperature the fluid reaches after the solar heat input, $T_{x'}$ (Fig. 7(c)) always increase with N and are larger for CO_2. Except for He, all numerical values are above 1000 K. Lowest values are reached for He. From the viewpoint of the solar receiver, this means that helium is a good refrigerant. Temperatures of the fluids after regeneration in the cold part of the cycle, T_y (Fig. 7(d)), are relatively high in all cases, although decrease with N. This makes feasible to combine the Brayton cycle with a bottoming one as a Rankine in order to take advantage of residual heat. This conclusion is valid for any working fluid.

Specific fuel consumption, m_f, assuming natural gas fueling is shown in Fig. 8. Fuel consumption is larger for He, specially for $N = 1$, where no regeneration is assumed. For N_2 and air, the model predicts about 135 kg/(MWh) for $N = 1$ and smaller values for larger N. The main reduction is got in the change from $N = 1$ to $N = 2$. In the case of CO_2,m_f is almost constant. Its numerical value is around 115 kg/(MWh). The fact that in all cases m_f decreases with N means that in spite of the fueling required by intermediate reheaters, the cycles takes advantage of regeneration. This is shown by the increasing behavior of the temperature of the fluids after regeneration in the heat absorption process, T_x (Fig. 7(b)).

5. Optimum pressure ratios for each fluid

Up to now the same pressure ratio for all fluids was assumed, particularly the experimental one of the gas turbine employed in project Solugas was chosen, $r_p = 9.9$. The aim of this section is to analyze simultaneously three ingredients in order to seek for optimum plant designs: working fluids, number of compression/expansion steps, and overall pressure ratio. Different efficiencies have been calculated considering the pressure ratio as a variable up to $r_p = 20$.

Overall plant efficiency is displayed in Fig. 9. In the case of He (Fig. 9(a)) two configurations were checked for $N = 1$, with and without regeneration. When regeneration is considered, optimum pressure ratios leading to the highest efficiencies are around $r_p = 4$, leading to $\eta \simeq 0.37$. Values of r_p above 8 leads to worse efficiencies than for the non-regenerative configurations. The incorporation of regeneration increases overall efficiency about 20%, provided that a lower value of the pressure ratio is considered.

For air and nitrogen the curves for η monotonically increase with r_p except for the single-stage configuration, where there is a quite flat maximum between values of r_p in the interval 6−10. In the case of CO_2 (Fig. 9(d)) always an increase of the pressure ratio leads to larger values of efficiency, although for $N = 1$,η is almost constant above $r_p \simeq 10$.

Fuel conversion rate, r_e, for all the working fluids, has a narrow maximum (see Fig. 10) for low values of r_p. For He (Fig. 10(a)) this maximum is below the values of r_e for multi-stage configurations. Curves of η and r_e are very similar due to the scarce solar heat input for this fluid with the considered aperture area. On the other side, for CO_2 (Fig. 10(d)), r_e for $N = 1$ is larger than for any other configuration and any other value of the pressure ratio ($r_e = 0.68$). Air and nitrogen are intermediate cases: values of r_e for $N = 1$ and low r_p are similar than those for multi-stage configurations and larger r_p values. For configurations with $N \geqslant 2$ there is a wide interval of values of r_p leading to good fuel conversion rates. Except for He, small r_p values lead to higher values of r_e for plant layouts with N small. As r_p increases an inversion point is reached (r_p between 6 and 8, depending on the fluid) from which higher N leads to higher values of r_p, *i.e.*, the increase on power output compensates the increase of fuel consumption.

Fig. 11 contains the evolution of the power output curves. These curves are always monotonic for multi-stage configurations. For $N = 1$, air and nitrogen display a shallow maximum about $r_p \simeq 10$. This point corresponds to the design point of Solugas project. Helium (Fig. 11(a)) shows a maximum for $r_p \simeq 5$.

Figures for the specific fuel consumption, m_f, are not shown because are essentially the reversal of those for r_e. The maxima turn to be minima and the increasing behavior of most curves with r_p turns to be decreasing. To have a numerical idea, minimum m_f is got for CO_2,$N = 1$ and $r_p = 5$,$m_f = 108$ kg/(MWh). For air and nitrogen minimum fuel consumption is reached at similar conditions and is about 120 kg/(MWh).

6. Predictions for two-stages compression cycles

In the previous section was shown that there exist a considerable increase on plant output records from single-stage configurations to two-stage configurations. The subsequent improvement for a higher number of compression/expansion steps is not so noticeable. Thus, in this section particular predictions for two different plant layouts with two compressors and intercooling ($N_c = 2$) are presented: two-stages expansion with reheating ($N_t = 2$) and single-stage expansion ($N_t = 1$). As a function of the pressure ratio, the overall plant efficiency, η, for each fluid is always smaller for single expansion (see Fig. 12(a)) than for two-stages expansion, irrespectively of the working fluid. But it is noteworthy that for air and nitrogen the curves in the case of $N_t = 1$ have a maximum around $r_p = 12$, whereas for $N_t = 2$ are monotonic in all the surveyed interval for r_p. In the case $N_t = 2$, overall efficiency can reach values slightly above 0.4 for air and nitrogen at $r_p \simeq 20$. For $N_t = 1$,η_{max} can be about 0.36–0.38, depending on the fluid (see Table 3 for precise values). The power block efficiency, η_h (Fig. 12(c)), can attain values around 0.5 for $N_t = 2$ and $r_p \simeq 20$, and 0.46 for air or nitrogen for $N_t = 1$ at $r_p \simeq 10$.

Fuel conversion efficiency, r_e (see Fig. 12(d)) behaves differently that overall efficiency. It is always larger (except for He) for $N_c = 2$,$N_t = 1$ than for $N_c = N_t = 2$. Carbon dioxide leads to the best values of fuel conversion efficiencies, specially for $N_c = 2$,$N_t = 1$ at low values of r_p and also gives reasonable good values of overall efficiency

and low specific fuel consumption (see also Fig. 13): $r_{e,max} = 0.70$ and $m_{f,min} = 108$ kg/(MW h). Comparing with air and nitrogen (that give similar numbers) in the same conditions, carbon dioxide improves fuel conversion efficiency by 7.7% and decreases specific fuel consumption by 8.5%. And comparing with the reference plant, Solugas, overall efficiency increases 18.7%, fuel conversion efficiency 22.8%, and specific fuel consumption diminishes 22.2%.

With respect to helium, in spite of the probably small size of the heliostat field taken from the reference plant, overall efficiency (Fig. 12(a)) could take values about 0.45 for $N_t = N_c = 2$ and $r_p = 8$, and about 0.40 for $N_t = 1, N_c = 2$ and $r_p = 5$. Fuel conversion rate (Fig. 12(d)) is expected to be around 0.40–0.45, that are numbers considerable smaller than those for air or carbon dioxide.

7. Conclusions

A general thermodynamic model for central tower hybrid Brayton thermosolar plants has been developed. The model is capable to predict overall plant performance and other records in terms of the efficiencies of plant subsystems: solar field and receiver, Brayton heat engine, and combustion chamber. Morevover, it allows to analyze multi-stage compression and expansion, and also recuperative or non-recuperative layouts. Temperature dependent specific heats of the working fluid are taken into account. Output records depend on a not large number of parameters with clear physical meaning, so it is feasible to develop sensitivity analysis and to propose optimum plant configurations.

Numerical results are presented for several working fluids, taking the size and data from a real prototype plant of about 5 MW at design conditions (*Solugas* project, Seville, Spain). First, a fixed overall pressure ratio is considered ($r_p = 9.9$) and four (gaseous) working fluids at subcritical conditions (dry air, nitrogen, carbon dioxide, and helium) analyzed for different multi-stage configurations. Two-stage compression and expansion configurations using air, nitrogen or CO_2 as working fluids are capable to increase overall plant efficiency about 17–20 % with respect to the reference plant (Solugas). In the case of helium, overall efficiency increases up to 40%, but large increase of fuel consumption due to reheaters between turbines is observed. In this case, the predicted solar share is small probably because the solar field taken as reference is undersized. For the other fluids, the increase of power output associated to multi-stage compression and expansion balances the increase of fuel consumption and so, the fuel conversion rate improves.

Afterwards an analysis of optimum plant configurations was presented. Three ingredients were analyzed together: the working fluid, the number of compression/expansion steps, and the overall pressure ratio. For single-stage layouts, the curves of the overall plant efficiency, η, when plotted against the pressure ratio, r_p, have a maximum between $r_p = 5–8$ except for CO_2. For multi-stage configurations, η increases monotonically with r_p for all fluids. The fuel conversion rate has a maximum for single-stage configurations at low values of pressure ratio, $r_p \simeq 4–5$. These maxima values are high, especially for subcritical CO_2.

An specific analysis for two-stages compression cycles ($N_c = 2$) including single-stage expansion ($N_t = 1$) and two-stages expansion ($N_t = 2$) was done. Overall efficiency is larger for $N_t = 2$, but this is opposite for the fuel conversion rate, r_e. The fluid leading to the highest values of r_e is again CO_2 with $N_c = 2$ and $N_t = 1$, that attains $r_e \simeq 0.7$ at $r_p \simeq 5$. Comparing with the data of the reference plant (*Solugas*, single-stage, and working with air at $r_p = 9.9$), overall efficiency increases 18.7%, fuel conversion rate increases about 22.8%, and specific fuel consumption decreases about 8.5%, leading to values about 108 kg/(MW h). These numbers suggest that the use of subcritical CO_2 with two compressors, intercooling, and single-stage expansion could be an interesting option for future plant designs.

Acknowledgements

Financial support from University of Salamanca and Junta de Castilla y León (project SA017P17) is acknowledged.

References

[1] Nathan GJ, Jafarian M, Dally BB, Saw WL, Ashman PJ, Hu E, et al. Solar thermal hybrids for combustion power plant: A growing opportunity. Prog Ener Comb Sci 2017;000:1–25.
[2] Peterseim JH, White S, Tadros A, Hellwig U. Concentrated solar power hybrid plants, which technologies are best suited for hybridisation? Renew Ener 2013;57:520–32.
[3] Powell KM, Rashid K, Ellingwood K, Tuttle J, Iverson BD. Hybrid concentrated solar thermal power systems: A review. Renew Sust Ener Rev 2017;80:215–37.
[4] Olumayegun O, Wang M, Kelsall G. Closed-cycle gas turbine for power generation: a state-of-the-art review. Fuel 2016;180:694–717.
[5] del Río A, Korzynietz R, Brioso JA, Gallas M, Ordoñez I, Quero M, et al. Soltrec – Pressurized volumetric solar air receiver technology. Energ Proc 2015;69:360–8.
[6] Ho CK, Iverson BD. Review of high-temperature central receiver designs for concentrating solar power. Renew Sust Energ Rev 2014;29:835–46.
[7] Korzynietz R, Brioso JA, del Río A, Quero M, Gallas M, Uhlig R, et al. Solugas – Comprehensive analysis of the solar hybrid Brayton plant. Sol Ener 2016;135:578–89.
[8] Dunham M, Iverson B. High-efficiency thermodynamic power cycles for concentrated solar power systems. Renew Sust Energ Rev 2014;30:758–70.
[9] Osorio JD, Hovsapian R, Ordonez JC. Dynamic analysis of concentrated solar supercritical CO_2-based power generation closed-loop cycle. Appl Therm Eng 2016;93:920–34.
[10] McMahan A, Klein S, Reindl D. A finite-time thermodynamic framework for optimizing solar-thermal power plants. J Sol Energ Eng 2007;129:355–62.
[11] Zare V, Hasanzadeh M. Energy and exergy analysis of a closed Brayton cycle-based combined cycle for solar power tower plants. Ener Conv Manage 2016;128:227–37.
[12] Barigozzi G, Bonetti G, Franchini G, Perdichizzi A, Ravelli S. Thermal performance prediction of a solar hybrid gas turbine. Sol Energy 2012;86:2116–27.
[13] Barigozzi G, Perdichizzi A, Gritti C, Guaiatelli I. Techno-economic analysis of gas turbine inlet air cooling for combined cycle power plant for different climatic conditions. Appl Therm Eng 2015;82:57–67.
[14] Milani D, Tri Luu M, McNaughton R, Abbas A. A comparative study of solar heliostat assisted supercritical CO_2 recompression Brayton cycles: Dynamic modelling and control strategies. J. Supercrit Fluids 2017;120:113–24.
[15] Kalathakis C, Aretakis N, Roumeliotis I, Alexiou A, Mathioudakis K. Concentrated solar power components toolbox in an object oriented environment. Sim Model Prac Theo 2017;70:21–35.
[16] Iverson B, Conboy T, Pasch J, Kruizenga A. Supercritical CO_2 Brayton cycles for solar-thermal energy. Appl Energ 2013;111:957–70.
[17] Al-Sulaiman F, Atif M. Performance comparison of different supercritical carbon dioxide Brayton cycles integrated with a solar power tower. Energy 2015;82:61–71.
[18] Luu MT, Milani D, McNaughton R, Abbas A. Dynamic modelling and start-up operation of a solar-assisted recompression supercritical CO_2 Brayton power cycle. Appl Ener 2017;199:247–63.
[19] Vasquez Padilla R, Soo Too Y, Benito R, McNaughton R, Stein W. Thermodynamic feasibility of alternative supercritical CO_2 Brayton cycles integrated with an ejector. Appl Ener 2016;169:49–62.
[20] Ahn Y, Bae SJ, Kim M, Cho S, Baik S, Cha JE. Review of supercritical CO_2 power cycle technology and current status of research and development. Nucl Eng Technol 2015;47:647–61.
[21] Reyes-Belmonte MA, Sebastián A, Romero M, González-Aguilar J. Optimization of a recompression supercritical carbon dioxide cycle for an innovative central receiver solar power plant. Energy 2016;112:17–27.
[22] Sánchez-Orgaz S, Medina A, Calvo Hernández A. Thermodynamic model and optimization of a multi-step irreversible Brayton cycle. Energ Convers Manage 2010;51:2134–43.
[23] Olivenza-León D, Medina A, Calvo Hernández A. Thermodynamic modeling of a hybrid solar gas-turbine power plant. Energ Convers Manage 2015;93:435–47.
[24] Sánchez-Orgaz S, Medina A, Calvo Hernández A. Recuperative solar-driven multi-step gas turbine power plants. Energ Convers Manage 2013;67:171–8.
[25] Santos MJ, Merchán RP, Medina A, Calvo Hernández A. Seasonal thermodynamic prediction of the performance of a hybrid solar gas-turbine power plant. Energ Convers Manage 2016;115:89–102.
[26] Quero M, Korzynietz R, Ebert M, Jiménez AA, del Río A, Brioso JA. Solugas – operation experience of the first solar hybrid gas turbine system at MW scale. Energ Proc 2014;49:1820–30.
[27] Heywood J. Internal combustion engine fundamentals. McGraw-Hill; 1988.
[28] Collado FJ, Turégano JA. Calculation of the annual thermal energy supplied by a defined heliostat field. Sol Ener 1989;42:149–65.
[29] López-Herraiz M, Bello Fernández A, Martinez N, Gallas M. Effect of the optical properties of the coating of a concentrated solar power central receiver on its thermal efficiency. Sol Energ Mat Sol Cells 2017;159:66–72.
[30] Duffie J, Beckman W. Solar engineering of thermal processes. Hoboken, New Jersey: John Wiley and Sons; 2006.
[31] Siva Reddy V, Kaushik SC, Tyagi SK. Exergetic analysis and economic evaluation of central tower receiver solar thermal power plant. Int J Ener Res 2014;38:1288–303. http://dx.doi.org/10.1002/er.3138.

[32] Solar, Turbines, Caterpillar. [link]. URL https://mysolar.cat.com/cda/files/126873/7/dsm50pg.pdf.
[33] Lemmon EW, Huber ML, McLinden MO. NIST Standard Reference Database 23: Reference fluid thermodynamic and transport properties-REFPROP, version 9.1, National Institute of Standards and Technology, Standard Reference Data Program, Gaithersburg; 2013.
[34] Najjar Y, Zaamout M. Comparative performance of closed cycle gas turbine engine with heat recovery using different gases. Heat Recovery Syst CHP 1992;12:489–95.
[35] No HC, Kim JH, Kim HM. A review of helium gas turbine technology for high temperature gas-cooled reactors. Nucl Eng Technol 2007;39:21.
[36] McDonald CF. Helium turbomachinery operating experience from gas turbine power plants and test facilities. App Therm Eng 2012;44.
[37] Crespi F, Gavagnin G, Sánchez D, Martínez GS. Supercritical carbon dioxide cycles for power generation. Appl Ener 2017;195:152–83.
[38] Coco-Enríquez L, Muñoz Antón J, Martínez-Val JM. New text comparison between CO_2 and other supercritical working fluids (ethane, Xe, CH_4 and N_2) in line-focusing solar power plants coupled to supercritical Brayton power cycles. Int J Hydrogen Ener 2017;42:17611–31.
[39] Chacartegui R, Muñoz de Escalona J, Sánchez D, Monje B, Sánchez T. Alternative cycles based on carbon dioxide for central receiver solar power. Appl Thermal Eng 2011;31:872–9.